

G. Di Mauro<sup>1</sup>, M. Guida<sup>1</sup>, G. Olivares<sup>2</sup>, L. M. Gomez<sup>2</sup>, R. Turco<sup>3</sup>, R. Tesser<sup>3</sup>, S. Mallardo<sup>4</sup>, G. Santagata<sup>4</sup>, P. Russo<sup>4</sup>

<sup>1</sup>Department of Industrial Engineering, University of Naples Federico II, Naples, IT

<sup>2</sup>Jerry Moran Center for Advanced Virtual Engineering & Testing (AVET), National Institute for Aviation Research (NIAR), Wichita State University (WSU), Kansas, US

<sup>3</sup>Department of Chemical Sciences, University of Naples Federico II, Naples, IT

<sup>4</sup>Institute of Polymers, Composites and Biomaterials (IPCB), National Research Council (CNR), Pozzuoli (NA), IT

### **Abstract**

In the context of global environmental sustainability initiatives, lithium-ion batteries have become the primary power source for a multitude of applications. Consequently, the aviation industry is increasingly exploring electrification as a potential solution to mitigate emissions and combat climate change. However, the widespread adoption of this technology is hampered by the limitations of conventional batteries, particularly their low specific and volumetric energy densities. This challenge justifies current research efforts on Structural Batteries, a novel technology designed to integrate energy storage and load-bearing functionalities within a single multifunctional material structure. This approach has the potential to significantly reduce the weight of electric airplanes.

This paper presents the design, manufacturing process, and promising initial performance of a prototype Structural Battery demonstrator. Furthermore, the importance of incorporating eco-design principles to ensure sustainable recycling at the battery's end-of-life is emphasized.

Keywords: Structural batteries, multi-functionality, preliminary assessment, composites

# 1. Introduction

for significant weight savings [4, 5].

The tuning of the batteries for various applications of the transport sector is an ambitious target. The pollutant emissions and mostly the process for battery recycling and recovery are peculiar aspects to consider for new energy storing system designs. With a particular focus on the aviation sector, the goal is to reduce the weight of conventional batteries, to obtain better performances in terms of specific and volumetric energy densities, limiting parameters for the spread of electric energy onboard aircraft if compared to the values reached by conventional energy sources. In detail, even if the most advanced current battery storage system is considered, worse performance than traditional fuels like Diesel and Kerosene are reached. Once the required energy is fixed, the weight of a lithium battery is about 60 times than that of a Kerosene tank and the required storage space itself is 18 times bigger. This is obviously a core issue, especially for the heavier aircraft categories, in which the energy request increases. Moreover, pollution remains a problem, since approximately 95% of lithium batteries are landfilled instead of recycled upon reaching end of life.

In this scenario a novel technology, named Structural Battery, has been conceived. Structural Batteries stand out as a possible solution to improve aircraft electric energy-storing capabilities, since they combine energy storage and load-bearing capabilities in multifunctional material structures, thus enabling electrification towards environmental friendliness of air transport. These are multifunctional components, manufactured similarly to composite materials already used on many aircraft, and capable of replacing stress-supporting parts typically made from metal alloys or carbon fibers [1-3]. The state of the art on this topic includes different research paths involving the study of the materials to be adopted for the different layers of the Structural Battery, the assembly, the scale-up, and the multiphysics modeling of this novel technology. The possible applications are endless, ranging from

the casings for mobile phones, to laptops, or structural components of cars and airplanes, allowing

Very sensitive is the airworthiness assessment of this novel technology, since it raises relevant issues about the requirements that need to be applied when considering multi-functional materials. To do so, with the collaboration of the National Research Council, in the context of a project promoted by Leonardo company, a Structural Battery model has been realized, accounting the information gathered from the literature State of the Art.

The Structural Battery demonstrator aims to achieve a gravimetric energy density between 40 and 50 Wh/kg, a nominal discharge rate of 1°C, being able to sustain more than 300 cycles at 0.1°C with 90% capacity retention.

The structural battery demonstrator consists of positive and negative electrodes, made of carbon fiber fabrics, already used for aeronautical applications, since characterized by high stiffness and strength, also allowing lithium ions intercalation by functionalizing it with active materials such as LiFePO<sub>4</sub>.

Considering that the electrical performance of the structural batteries depends on various factors, such as the degree of adhesion of the salt to the carbonaceous substrate and the level of salt that binds to its substrate, various lithium salts that can obtain good quantities of deposited lithium on carbon fiber substrates have been investigated. Their effectiveness is monitored by specific surface characterization techniques such as SEM-EDAX morphological studies.

The functionalization process has been performed by spray coating a solution capable of solubilizing LiFePO<sub>4</sub> onto the carbon fiber fabrics, first activated by plasma treatment to improve surface wettability by promoting intense and stable adhesion of lithium ions over time.

For the sake of completeness, the adopted Structural battery configuration is shown in Figure 1, together with the first manufactured demonstrator.

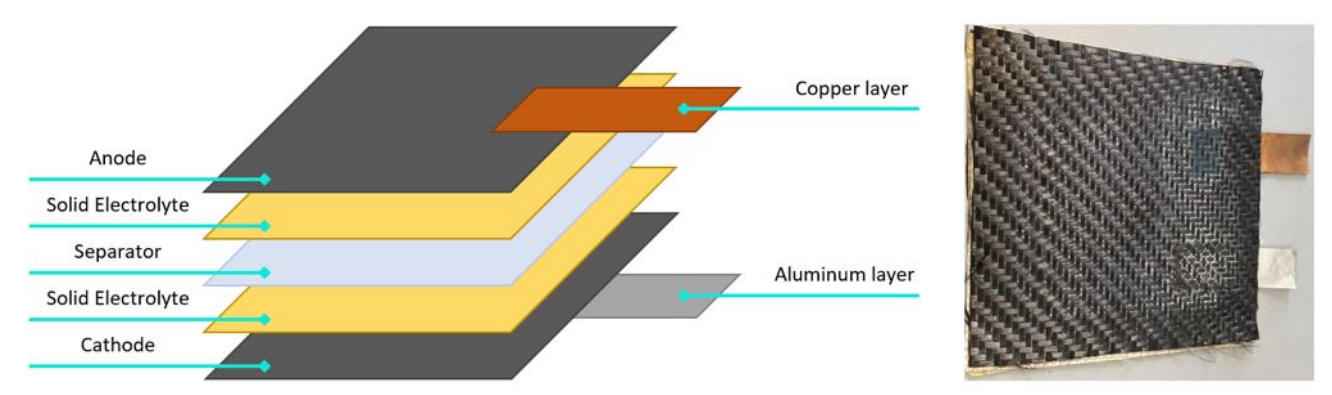


Figure 1 - Schematization and first manufactured demonstrator of the proposed Structural Battery configuration.

In this activity, along with the breakdown of the adopted manufacturing process, the concept of ecodesign is emphasized, since the Structural Battery is conceived in a configuration such that when it reaches its end of life, the recycling and component recovery process is completely sustainable.

Attention is dedicated to the combination of the different layers for the Structural Battery, performed by hand layering them and compacting the stacked system using a hydraulic laboratory press. The considered process conditions have been set based on the decades of prior experience of the IPCB resources involved in the project regarding the development of thermoplastic composite structural laminates.

A special focus is dedicated to the Solid Polymer Electrolyte (SPE) layers, fundamental to get a Structural Battery capable to storage electric energy and carry loads. They have been made by polypropylene, typically used as a matrix in thermoplastic composite structural laminates, in which electrical percolation conditions are reached by dispersing lithium salts. Such ingredients have been melted and mixed and the product compression moulded into thin films to use as lithium conductive layers inserted in the anode and cathode portions of the structural battery. In detail, different formulations for the SPE layers have been manufactured and preliminarily characterized by structural (FTIR-ATR), thermal (DSC, TGA), morphological (SEM) and mechanical (tensile tests) analysis.

## 2. Electrolyte in the Solid State

PEO-based SPEs have been manufactured using PEG of different molecular weight, PEG 1000 (1400-1600 g/mol) and PEG 1550 (1400-1600 g/mol) of analytical grade, PEO, SEP and lithium triflate (LiCF<sub>3</sub>SO<sub>3</sub>). Organo-modified sepiolite (SEP<sub>mod</sub>) was prepared by suspending 5 g of SEP in 100 mL of deionized water containing 5% or 10% (w/w) of both PEG under homogenization with an UltraTurrax IKA T25 disperser at 12,000 rpm for 15 minutes. The suspension was then washed and centrifuged three times, and the recovered solid fraction was dried under vacuum at 40°C overnight. Physical blends of SEP<sub>mod</sub>, PEO and LiCF<sub>3</sub>SO<sub>3</sub> were prepared through solvent-free melt blending using a Brabender Plasti-Corder internal mixer at 140°C and 80 rpm for 20 minutes. The results were cooled at room temperature and then ground by a centrifugal bladed mill Retsch ZM1. The obtained powders were dried under vacuum at 40°C for 24 hours, and then ground and dried again. Finally, films were prepared using a hot press at 130°C: first applying no pressure for 5 minutes to remove entanglements, then 20 bar for 2 minutes to allow homogeneous melting, and finally 40 bar for 2 minutes for optimization of salt and clay distribution. A water quench for 10 minutes brought the films to room temperature. The entire manufacturing process is schematized in Figure 3, while the identification codes (ICs) along with the composition of the formulations adopted for the PEO-based SPE films are detailed in Table 1.

		expressed in percentage.

IC	PEO	LiCF <sub>3</sub> SO <sub>3</sub>	SEP	PEG 1000	PEG 1550
SPELi	91.5	8.5	/	/	/
SPE <sub>0</sub>	87.5	8.13	4.36	/	/
SPE₁	87.5	8.13	4.15	/	0.21
SPE <sub>2</sub>	87.5	8.13	4.15	0.21	/
SPE <sub>3</sub>	87.5	8.13	3.96	/	0.40
SPE <sub>4</sub>	87.5	8.13	3.96	0.40	/



Figure 2 - Processing steps of the SPE films preparation.

The compression-molded films, together with neat material samples (PEO, PEG, and SEP), have been subjected to different tests. Attenuated total reflection Fourier-transform infrared (ATR-FTIR) spectroscopic analyses were performed as shown in Figure 3.

The analysis involved surface mapping of different areas per film at room temperature, with an average of 16 scans and a resolution of 4 cm<sup>-1</sup> in the range of 4000-650 cm<sup>-1</sup>.

The spectra of PEG and PEO overlap due to their identical chemical structures and functional groups, so only the PEO functional groups were considered. The characteristic absorption bands of PEO have

been detailed, with peaks at various wavelengths corresponding to different types of stretching, bending, and twisting vibrations. These vibrations confirm the semi-crystalline nature of the polymer [6, 7]. FTIR-ATR absorption peaks of PEO are highlighted, corresponding to various types of vibrations, including Mg-OH, coordinated water, zeolitic water, Si-O stretching, O-H deformation, and Mg-OH bending [8, 9].

It results that SEP forms a checkerboard pattern with tunnels containing structural water molecules, which grants it excellent adsorptive properties relevant for SPE production [10-12]. The spectra of LiCF<sub>3</sub>SO<sub>3</sub> have been also analysed, with peaks at various wavelengths corresponding to different types of vibrations [13].

The analysis of the spectra suggests potential physical interactions between PEO, PEG, and SEP<sub>mod</sub>. However, attributing conformational changes to specific interactions within these complex structures is challenging.

In the high-frequency region, notable differences have been found between unmodified sepiolite and SPE<sub>0</sub>/SPE<sub>4</sub> films. The coordinated water and zeolitic water peaks in plain SEP significantly change conformation in the films, likely due to hydrogen bonds formed with clay mineral surfaces. The presence of lithium ions and polar residues from the SPE<sub>0</sub> polymer matrix and SPE<sub>4</sub> film PEG plasticizer also likely contribute to these interactions.

Changes in the bending vibration region and salt stretching deformations also confirm interactions between sepiolite, salt, and polymers. The merging of peaks related to PEO crystalline phase methylene group wagging and CH<sub>2</sub> symmetric and asymmetric twisting modes in SPE films suggests that both LiCF<sub>3</sub>SO<sub>3</sub> and SEP influenced PEO crystallinity. The silicate absorption peak is also present, suggesting physical interaction between the polymer matrix and SEP silicate fractions [14-17].

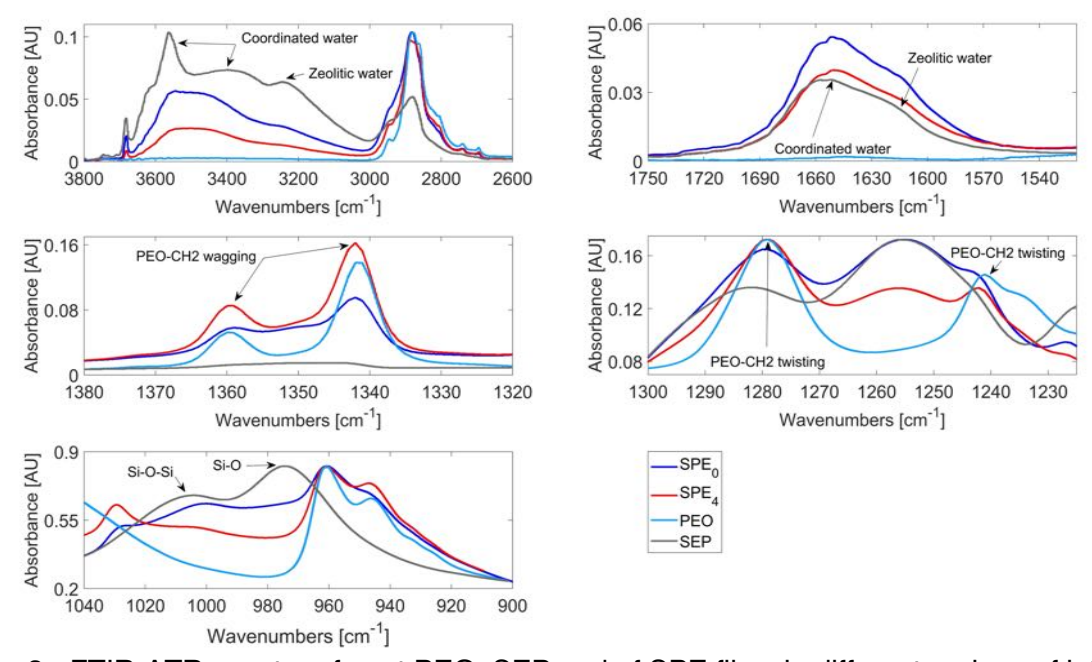


Figure 3 - FTIR-ATR spectra of neat PEO, SEP and of SPE films in different regions of interest.

Differential Scanning Calorimetry (DSC) have been adopted to investigate the crystallization and melting behavior of compression-molded samples, along with neat PEO, PEG 1000, and PEG 1500 SEP samples. The samples were subjected to a thermal cycle from 25°C to 250°C under an inert liquid nitrogen atmosphere, with a 1-minute isothermal step and a non-isothermal crystallization cooling at 50°C/min to -80°C. Results are shown in Figure 4. All samples started crystallization at significantly low temperatures due to the rapid cooling rate employed, which reflects industrial cooling practices [18]. Rapid cooling hinders chain entanglement and promotes an amorphous-frozen state in the solid. Polymer crystallinity significantly influences macroscopic properties such as mechanical performance [19, 20], and the presence of additives within semi-crystalline polymers can alter their crystallization and melting behavior [21, 22].

All doped samples (including sepiolite, lithium salt, and PEG) started crystallization before neat PEO

and SPE0, due to the combined nucleating and plasticizing effects of the additives. SPE<sub>2</sub> exhibited the fastest crystallization due to the balanced nucleating and plasticizing action of PEG 1000. Lower molecular weight and amount of plasticizer reduced PEO intermolecular forces, enhancing free volume and chain mobility, favoring crystallization.

Significant differences were observed between doped blends, neat PEO, and SPE<sub>0</sub>. Neat PEO exhibited slower crystallization due to the absence of nucleating agents or plasticizers, while SPE<sub>0</sub> showed distinct thermal behavior due to the absence of PEG. SEP lacks the PEG plasticizing effect and instead delays PEO macromolecular organization at low temperatures, leading to non-crystalline PEO conformations near the sepiolite surfaces [23].

DSC curves related to the second heating ramp showed that all investigated systems, except the neat polymer, exhibited similar melting temperatures and profiles, indicating a regular endothermic peak likely associated with the melting of well-defined crystalline structures formed during cooling [24]. Table 2 showed a general trend of increasing crystallinity percentage, likely due to the formation of tighter structures through physical interactions between the polymer, salt, PEG, and sepiolite. SPE<sub>2</sub> and SPE<sub>3</sub> exhibited the highest crystallinity values, which aligns with their high ΔH<sub>m</sub> values, strongly correlated to physical entanglements within the blend developed during melt crystallization [25].

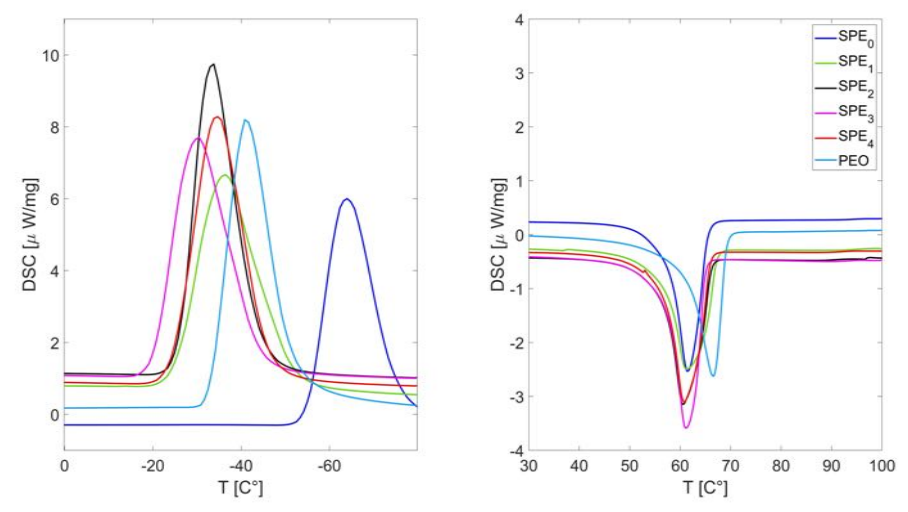


Figure 4 - Melt crystallization (left) and second heating run (right) of plain PEO and SPE based films.

Thermogravimetric (TG) and derivative thermogravimetric (DTG) analyses have been considered to investigate the thermal stability of solid polymer electrolyte (SPE) films. The analyses were conducted using a Perkin-Elmer Pyris Diamond TGA/DTG analyzer, with samples heated from 25 °C to 600 °C at 10 °C/min under nitrogen flow. The TG and DTG curves of the SPE films (Figure 5) showed a single major weight loss step, followed by lithium triflate degradation at higher temperatures. All SPE systems displayed enhanced thermal stability compared to neat PEO, due to the inclusion of reinforcing and stabilizing agents within the polymer matrix.

In SPE<sub>0</sub>, SPE<sub>1</sub>, SPE<sub>2</sub>, and SPE<sub>3</sub>, polymer degradation started at higher temperatures and extended to 450°C, due to the dominant reinforcing effect of sepiolite [26]. This suggested tight intermolecular entanglements between components, leading to mutual stabilization. The single sharp degradation patterns in both TG and DTG curves indicated good physical compatibility within the blends.

Conversely, SPE<sub>4</sub> was significantly influenced by the high PEG 1000 concentration, causing a shift in the entire thermal degradation profile towards lower temperatures due to the prevailing plasticizing effect [27].

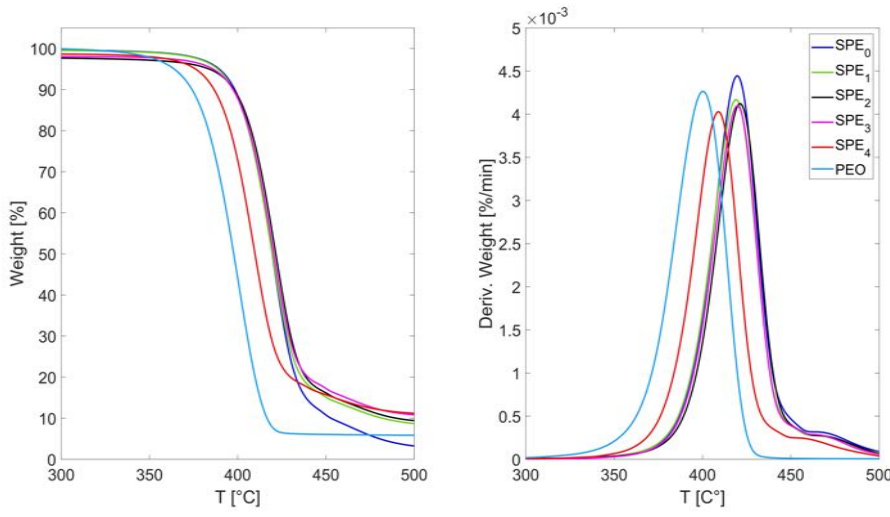


Figure 5 - TGA (left) and DTG (right) of PEO and SPE based films under nitrogen.

Table 2 - Thermal parameters of SPE based films and neat polymers measured by DSC and TGA analysis. The values of crystallization and melting enthalpy in parentheses ( $\Delta H$ ) and the crystallinity ( $\chi$ ) are normalized with respect to the weight fraction of the polymer in the blend.

	ΔH <sub>c</sub> [J/g]	T <sub>c,onset</sub> [°C]	T <sub>c</sub> [°C]	$\Delta H_m[J/g]$	T <sub>m</sub> [°C]	T <sub>onset</sub> [°C]	T <sub>peak</sub> [°C]	X <sub>c</sub> [%]
	± 2%	± 2%	± 2%	± 1%	± 2%	± 2%	± 2%	
PEO	146.9	-31.7	-40.6	121.8	66.4	366.7	400.2	59.4
SPE <sub>0</sub>	118.2	-51.7	-64.0	117.4	62.4	391.9	419.7	65.4
SPE <sub>1</sub>	117.4	-21.7	-36.4	118.4	61.3	388.7	419.0	66.0
SPE <sub>2</sub>	140.7	-18.3	-30.5	133.5	60.5	383.8	421.3	74.4
SPE <sub>3</sub>	119.2	-22.5	-33.8	136.1	61.2	386.	419.8	75.9
SPE <sub>4</sub>	134.3	-20.8	-34.4	123.8	60.9	376.1	409.0	69.0

Scanning electron microscopy (SEM) was used to analyze the morphology of the samples, which were sputter-coated with a gold-palladium alloy layer before observation. The micrographs were acquired at room temperature under high vacuum conditions.

Figure 6 shows the results of the SEM analysis. The SPE<sub>0</sub> sample (Figure 6a) has a non-uniform and highly structured polymer surface with fine and homogenous distribution of rod-like sepiolite filler domains. The presence of PEG plasticizers alters the polymer surface morphology. SPE<sub>1</sub> (Figure 6b) has a homogeneous, smooth, and continuous polymer surface with very fine sepiolite particles dispersed amongst the polymer chains [28]. In contrast, SPE<sub>2</sub> (Figure 6c) has a distinct surface topography, with a continuous but roughened polymer surface and good interfacial adhesion between the polymer matrix and plasticizer. The polymer interaction appears to influence the surface morphology's crystalline pattern, with a tightly packed and robust texture of the macromolecular chain distribution. Well-dispersed and well-embedded sepiolite particles are also observed in SPE<sub>2</sub>.

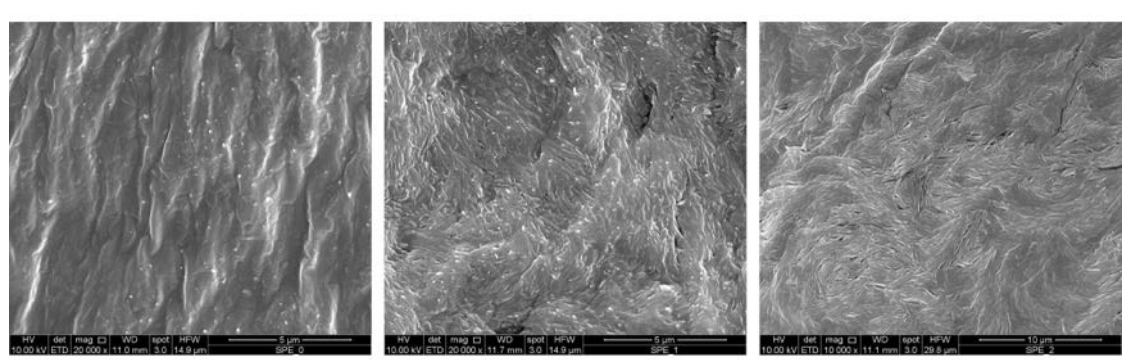


Figure 6 - SEM micrographs of SPE<sub>0</sub> (left), SPE<sub>1</sub> (center) and SPE<sub>2</sub> (right) surfaces.

In addition, tensile tests (Figure 7) were conducted on dumbbell-shaped film specimens using an Instron 4301 dynamometer. The tests were performed at 23  $\pm$  2 °C, 45  $\pm$  5% relative humidity, and a crosshead speed of 2 mm/min. Thickness (t), Young's modulus (E), failure stress ( $\sigma_f$ ), and strain ( $\epsilon_f$ ) were determined as average values of six measurements (Table 3).

The addition of lithium salt generally reduced mechanical properties compared to other PEO-based compositions. The SPE<sub>Li</sub> system, containing only PEO and lithium salt, exhibited the lowest elastic modulus due to the absence of inorganic filler. The lack of sepiolite in SPE<sub>Li</sub> led to a significant decrease in the Young Modulus and detrimental values for failure strain [29].

Except for the SPE<sub>1</sub> formulation, other SPE-based composites showed increased tensile stiffness with plasticizer addition, contrary to initial expectations. This is likely due to the increased flexibility induced by the plasticizer promoting greater crystallinity within the PEO matrix. Both plasticizers increased tensile strength, with a more pronounced effect for PEG 1000 compared to PEG 1550.

The mean values of failure stress decreased monotonically as the PEG 1550 content increases, while an opposite effect was observed in the presence of PEG 1000. The observed trends can be attributed to the interplay between increased matrix chain flexibility and the nucleating action of sepiolite. Failure strain also reflected the plasticizer influence on crystallinity, with formulations containing PEG 1550 showing an increase in strain for a plasticizer content equal to 0.21 wt.% and then a slight decrease for higher contents, while formulations with PEG 1000 displayed an exactly reversed trend.

Table 3 - Tensile test	parameters for each	adopted formulation
	parameters for each	i aaoptoa ioiiiiaiatioii.

Sample	t [mm]	E [MPa]	ε <sub>f</sub> [%]	σ <sub>f</sub> [MPa]
SPELi	0.092	99.0±13.27	3.5±0.4	1.1±0.2
SPE <sub>0</sub>	0.130	$331.7 \pm 30.0$	$4.5 \pm 07$	$1.2 \pm 0.1$
SPE <sub>1</sub>	0.145	305.6 ± 13.1	$5.9 \pm 2.6$	1.1 ± 0.4
SPE <sub>2</sub>	0.130	$343.8 \pm 10.8$	$4.8 \pm 0.8$	$1.2 \pm 0.2$
SPE <sub>3</sub>	0.148	397.9 ± 46.9	$6.4 \pm 1.5$	$0.8 \pm 0.5$
SPE <sub>4</sub>	0.103	426.4 ± 65.3	$3.8 \pm 0.4$	1.9 ± 0.1

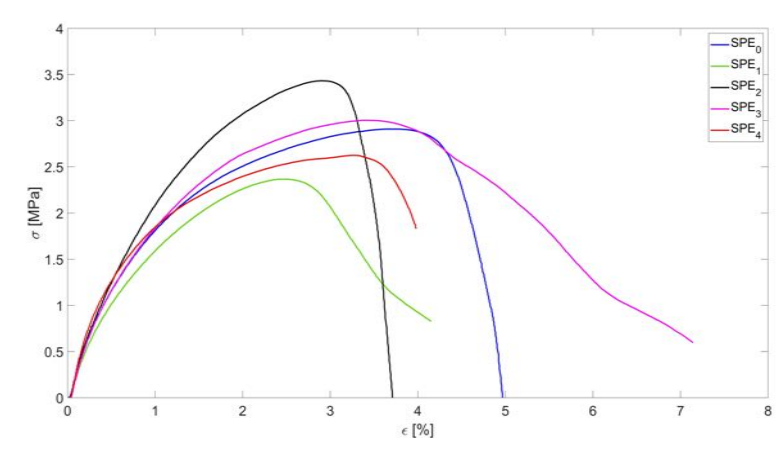


Figure 7 - Stress-strain curves for each adopted formulation.

## 3. Functionalization of the Cathode

The performance of the functionalized cathode to be included in the theorized SB configuration is reported. Multiple attempts have been made to deposit LiFePO<sub>4</sub> particles on a Carbon Fiber (CF) fabric with an innovative technique, namely spray coating combined with pretreatment by plasma technique. The latter improves the chemical and physical surface properties of the fabric by increasing its adhesion. Both original fabric and the functionalized one were then characterized by TGA and SEM analyses.

To deposit LiFePO<sub>4</sub> on the CF fabrics, it was planned to dissolve the latter within a solution. Numerous

attempts were made to identify which solution was suitable. A first attempt was made using only distilled water, as it would have been the greenest solution. The attempt reported negative results as LiFePO<sub>4</sub> precipitated instantly. The other attempts were made with acid-type solutions, to increase the chances of dissolving LiFePO<sub>4</sub>. Therefore, solutions containing HNO<sub>3</sub>, HCl, and H<sub>2</sub>SO<sub>4</sub> with different molar combinations have been considered. Figure 8 shows the preparation process for the solution containing LiFePO<sub>4</sub> used to impregnate the CF fabrics, in which the gradual change in the solution color is shown.







Figure 8 - Steps in the preparation of the solution chosen for CF tissue impregnation: solution of HNO<sub>3</sub>, HCl and H<sub>2</sub>SO<sub>4</sub> (left), LiFePO<sub>4</sub> addition (center) and dissolution (right).

Therefore, the solution was spray coated on the CF fabric, both as-is or pretreated by plasma technique, as showed in Figure 9. Plasma treatment was carried out on CF fabrics to improve surface wettability and roughness over time [30, 31]. The as-is CF fabric exhibits significant thermal stability, which is reflected by a 3% weight loss at 600°C. The fabric impregnated with LiFePO<sub>4</sub> without plasma pretreatment exhibits a 5% weight loss at 450°C, whereas the pretreated CF fabric exhibits greater thermal stability since it showed an 8% weight loss at 525°C, which is an indication that the solution has stabilized the fabric. Figure 9 also shows the TGA profile for the LiFePO<sub>4</sub>. It exhibits a weight loss greater than 85% at 600°C, indicating that all the weight loss observable in the impregnated CF fabrics is attributable to the salt itself.

Figure 10 presents the outcomes of the SEM analyses, validating the efficacy of the plasma treatment technique. The comparison among the untreated CF sample, the CF sample with direct LiFePO<sub>4</sub> deposition, and the plasma pretreated one is illustrated. Notably, the untreated CF sample is visibly free from any particles, whereas the CF sample with direct LiFePO<sub>4</sub> deposition displays white dots, indicating the successful adherence of LiFePO<sub>4</sub> particles on the fabric itself. Finally, the plasma pretreated CF sample reveals an increased number of LiFePO<sub>4</sub> particles deposited on its surface, substantiating the effectiveness of the applied treatment.

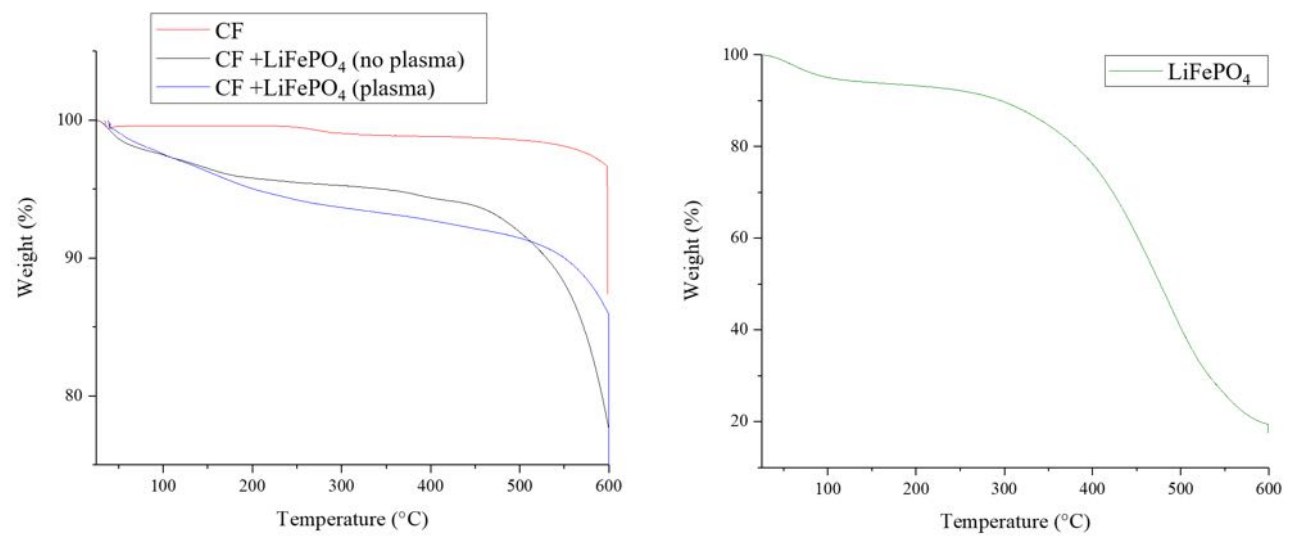


Figure 9 - TGA profiles for CF fabrics, both as-is or spray coated (left) and for LiFePO<sub>4</sub> (right).

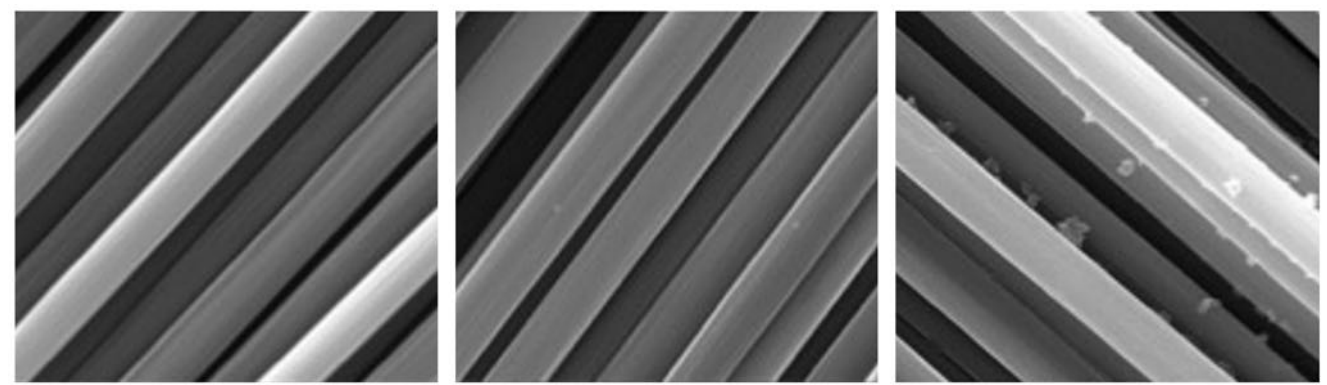


Figure 10 - SEM micrographs of the CF sample (left), the CF sample with direct LiFePO4 deposition (center), and the plasma pretreated one (right).

# 4. Assembly of the Structural Battery Demonstrator

The assembly of the Structural Battery demonstrator involved compacting the various components, as depicted in the exploded view in Figure 11. The compaction was performed using a hydraulic press set at a temperature of 60°C, following a predetermined pressure profile.

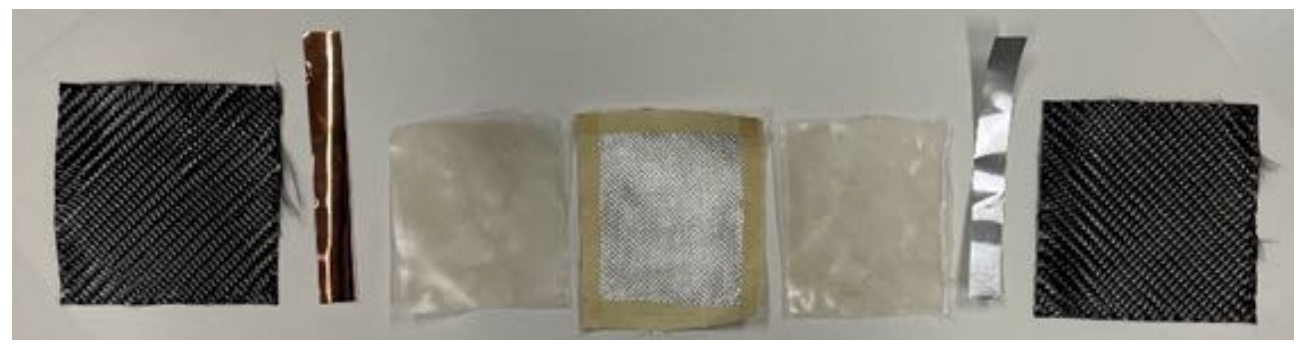


Figure 11 – Breakdown view of the Structural Battery components.

Upon assembly, the potential difference (ddp) of the battery was measured by connecting the current collectors of the demonstrator to a digital multimeter. A voltage value of 205 mV was recorded, as shown in Figure 12. The battery was then connected to a DC generator with a current of 100  $\mu$ A. After a charging time of 10 minutes, a ddp value of 1.2V was observed.



Figure 12 – First voltage measurement for the SB demonstrator.

The charging current was gradually increased, and the battery reached a maximum ddp value of 2.6V. An LED was then connected to SB current collectors to confirm its functionality, as shown in Figure 13

However, during the compaction process, partial leakage of the solid-state electrolyte layer was observed from the central area of the demonstrator, where contact between the electrodes was likely to occur, resulting in short-circuiting phenomena. To address this issue, adhesive tape was applied to the ends of the electrodes. This modification significantly improved the ddp stability.



Figure 13 – LED connecting to SB current collectors confirming its functionality.

## 5. Conclusions

This study focused on the development and characterization of solid polymer electrolyte films using PEO as the polymer matrix, PEG with varying molecular weights as plasticizers, SEP as a mineral carrier for salt ions, and lithium triflate as the inorganic electrolyte. The study explored diverse material compositions by modifying the PEG content while keeping PEO and lithium triflate constant.

Thermal, structural, morphological, and mechanical analyses reveal promising characteristics for the use of SPE films in structural batteries. The properties of the different blend compositions, such as polymer plasticization, thermal stability, mechanical rigidity, toughness, and flexibility, can be modulated through specific hydrogen bonding between the polar residues of polymers, SEP<sub>mod</sub> surface and channels, and lithium ions.

Notably, the one-pot solution processing via melt mixing and compression molding offers a sustainable, eco-friendly, cost-effective, and scalable approach for SPE fabrication.

Furthermore, several solutions were prepared to obtain a mixture capable of solubilizing LiFePO<sub>4</sub>. On the CF fabric surface. Coating with different solutions containing LiFePO<sub>4</sub> was performed by means

of spray coating process. To make the CF surface more hydrophilic, plasma treatment was used. Both as-is and functionalized CF surfaces were characterized by thermogravimetric and morphological analysis. The samples showed different properties attributable to the presence and relative amount of LiFePO<sub>4</sub>. However, further electrochemical investigations, such as impedance and cyclic voltammetry measurements, are necessary to verify the amount of LiFePO<sub>4</sub> deposited on the tissue and whether it is sufficient for the functionalized sample to have an adequate specific capacity.

## **Contact Author Email Address**

gennaro.dimauro@unina.it (corresponding author)
michele.guida@unina.it
luismanuel@niar.wichita.edu
gerardo.olivares@wichita.edu
rosa.turco@unina.it
riccardo.tesser@unina.it
salvatore.mallardo@ipcb.cnr.it
gabriella.saltagata@ipcb.cnr.it
pietro.russo@ipcb.cnr.it

# 6. Copyright Statement

The authors confirm that they, and/or their company or organization, hold copyright on all the original material included in this paper. The authors also confirm that they have obtained permission, from the copyright holder of any third-party material included in this paper, to publish it as part of their paper. The authors confirm that they give permission or have obtained permission from the copyright holder of this paper, for the publication and distribution of this paper as part of the ICAS proceedings or as individual off-prints from the proceedings.

# References

- [1] Di Mauro G, Corcione S, Cusati V, Marciello V, Guida M, Nicolosi F. The Potential of Structural Batteries for Commuter Aircraft Hybridization. *Journal of Materials Engineering and Performance*, Vol. 9, 32, pp 3871-3880, 2023.
- [2] Asp L E, Johansson M, Lindbergh G, Xu J, Zenkert D. Structural battery composites: a review. *Functional Composites and Structures*, Vol. 4, 1, pp 042001, 2019.
- [3] Kühnelt H, Beutl A, Mastropierro F, Laurin F, Willrodt S, Bismarck A, Romano F. Structural Batteries for Aeronautic Applications State of the Art, Research Gaps and Technology Development Needs. *Aerospace*, Vol. 1, 9, pp 7, 2021.
- [4] Blomgren G E. The development and future of lithium-ion batteries. *Journal of The Electrochemical Society*, Vol. 1, 164, pp A5019, 2016.
- [5] Adenusi H, Chass G A, Passerini S, Tian K V, Chen G. Lithium batteries and the solid electrolyte interphase (SEI) Progress and outlook. *Advanced Energy Materials*, Vol. 10, 13, pp 2203307, 2023.
- [6] Waly A L, Abdelghany A M, Tarabiah A E. Study the structure of selenium modified polyethylene oxide/polyvinyl alcohol (PEO/PVA) polymer blend. *Journal of Materials Research and Technology*, Vol. 14, pp 2962-2969, 2021.
- [7] Sahu M, Reddy V R M, Kim B, Patro B, Park C, Kim W K, Sharma P. Fabrication of Cu2ZnSnS4 light absorber using a cost-effective mechanochemical method for photovoltaic applications. Materials, Vol. 5, 15, pp 1708, 2022.
- [8] Farmer V C. The Infrared Spectra of Minerals. *Mineralogical society monograph*, Vol. 4, pp 331-363, 1974
- [9] Cornejo J, Hermosin M C. Structural alteration of sepiolite by dry grinding. *Clay Minerals*, Vol. 4, 23, pp 391-398, 1988.

- [10] Walczyk A, Karcz R, Kryściak-Czerwenka J, Napruszewska B D, Duraczyńska D, Michalik A, Serwicka, E M. Influence of Dry Milling on Phase Transformation of Sepiolite upon Alkali Activation: Implications for Textural, Catalytic and Sorptive Properties. *Materials*, Vol. 18, 13, pp 3936, 2020.
- [11]Kuang W, Facey G A, Detellier C. Organo-mineral nanohybrids. Incorporation, coordination and structuration role of acetone molecules in the tunnels of sepiolite. *Journal of Materials Chemistry*, Vol. 2, 16, pp 179-185, 2006.
- [12] Arya A, Sharma A L. Polymer electrolyte for lithium-ion batteries: a critical study. *Ionics*, Vol. 3, 23, pp 497-540, 2017.
- [13]Kumar R, Sharma J P, Sekhon S S. FTIR study of ion dissociation in PMMA based gel electrolytes containing ammonium triflate: Role of dielectric constant of solvent. *European Polymer Journal*, Vol. 11, 41, pp 2718-2725, 2005.
- [14]Bregante D T, Chan M C, Tan J Z, Ayla E Z, Nicholas C P, Shukla D, Flaherty D W. The shape of water in zeolites and its impact on epoxidation catalysis. *Nature Catalysis*, Vol. 9, 4, pp 797-808, 2021.
- [15]Ruiz-Hitzky E. Molecular access to intracrystalline tunnels of sepiolite Basis of a presentation given at Materials Discussion. *Journal of Materials Chemistry*, Vol. 1, 11, pp 86-91, 2001.
- [16]Mora M, López M I, Carmona M Á, Jiménez-Sanchidrián C, Ruiz J R. Study of the thermal decomposition of a sepiolite by mid-and near-infrared spectroscopies. *Polyhedron*, Vol. 16, 29, pp 3046-3051, 2010.
- [17]Kim K, Kuhn L, Alabugin I V, Hallinan Jr D T. Lithium salt dissociation in diblock copolymer electrolyte using fourier transform infrared spectroscopy. *Frontiers in Energy Research*, Vol. 8, pp 569442, 2020.
- [18] Lewis O G. Physical constants of linear homopolymers. Springer Science & Business Media, 1986.
- [19]Kong Y, Hay J N. The measurement of the crystallinity of polymers by DSC. *Polymer*, Vol. 14, 43, pp 3873-3878, 2002.
- [20]Kong Y, Hay J N. The enthalpy of fusion and degree of crystallinity of polymers as measured by DSC. *European Polymer Journal*, Vol. 8, 39, pp 1721-1727, 2003.
- [21]Madbouly S A, Wolf B A. Crystallization kinetics of poly (ethylene oxide) from its melt and from mixtures with tetrahydronaphthalene and oligo (ethylene oxide-block-dimethylsiloxane). *Journal of Polymer Science Part B: Polymer Physics*, Vol. 5, 42, pp 820-829, 2004.
- [22]Kovacs A J, Straupe C. Isothermal growth, thickening and melting of poly (ethylene-oxide) single crystals in the bulk: III. Bilayer crystals and the effect of chain ends. *Journal of Crystal Growth*, Vol. 2, 48, pp 210-226, 1980.
- [23] Strawhecker K E, Manias E. Crystallization behavior of poly (ethylene oxide) in the presence of Na+montmorillonite fillers. *Chemistry of Materials*, Vol. 4, 15, pp 844-849, 2003.
- [24] Ibrahim S, Yasin S M M, Nee N M, Ahmad R, Johan M R. Conductivity, thermal and infrared studies on plasticized polymer electrolytes with carbon nanotubes as filler. *Journal of Non-Crystalline Solids*, Vol. 2, 358, pp 210-216, 2012.
- [25]Singh N K, Verma M L, Minakshi M. PEO nanocomposite polymer electrolyte for solid state symmetric capacitors. *Bulletin of Materials Science*, Vol. 38, pp 1577-1588, 2015.
- [26]Ramesh S, Wen L C. Investigation on the effects of addition of SiO 2 nanoparticles on ionic conductivity, FTIR, and thermal properties of nanocomposite PMMA–LiCF3SO3–SiO 2. *Ionics*, Vol. 16, pp 255-262, 2010.
- [27]Mejía A, García N, Guzmán J, Tiemblo P. Surface modification of sepiolite nanofibers with PEG based compounds to prepare polymer electrolytes. *Applied clay science*, Vol. 95, pp 265-274, 2014.
- [28]de Matos Costa A R, Crocitti A, Hecker de Carvalho L, Carroccio S C, Cerruti P, Santagata G. Properties of biodegradable films based on poly (butylene succinate) (PBS) and poly (butylene adipate-coterephthalate) (PBAT) blends. *Polymers*, Vol. 10, 12, pp 2317, 2020.
- [29]Klongkan S, Pumchusak J. Effects of the addition of LiCF3SO3 salt on the conductivity, thermal and mechanical properties of PEO-LiCF3SO3 solid polymer electrolyte. *International Journal of Chemical Engineering and Applications*, Vol. 3, 6, pp 165, 2015.

- [30]Dighton C, Rezai A, Ogin S L, Watts J F. Atmospheric plasma treatment of CFRP composites to enhance structural bonding investigated using surface analytical techniques. *International Journal of Adhesion and Adhesives*, Vol. 91, pp 142-149, 2019.
- [31]Jordá-Vilaplana A, Fombuena V, García-García D, Samper M D, Sánchez-Nácher L. Surface modification of polylactic acid (PLA) by air atmospheric plasma treatment. *European polymer journal*, Vol. 58, pp 23-33, 2014.